Astronomy & Astrophysics

LETTER TO THE EDITOR

Near-infrared detection and characterization of the exoplanet HD 95086 b with the Gemini Planet Imager[⋆]

R. Galicher[1], J. Rameau[2], M. Bonnefoy[2], J.-L. Baudino[1], T. Currie[3], A. Boccaletti[1], G. Chauvin[2], A.-M. Lagrange[2], and C. Marois[4]

[1] LESIA, CNRS, Observatoire de Paris, Univ. Paris Diderot, UPMC, 5 place Jules Janssen, 92190 Meudon, France
  e-mail: raphael.galicher@obspm.fr
[2] UJF-Grenoble 1/CNRS-INSU, Institut de Planétologie et d'Astrophysique de Grenoble (IPAG) UMR 5274, 38041 Grenoble, France
[3] Department of Astronomy and Astrophysics, Univ. of Toronto, 50 St. George St., Toronto M5S 1A1, Canada
[4] National Research Council of Canada Herzberg, 5071 West Saanich Road, Victoria V9E 2E7, Canada

ABSTRACT

HD 95086 is an intermediate-mass debris-disk-bearing star. VLT/NaCo 3.8 μm observations revealed it hosts a $5 \pm 2\,M_{\rm Jup}$ companion (HD 95086 b) at $\simeq$56 AU. Follow-up observations at 1.66 and 2.18 μm yielded a null detection, suggesting extremely red colors for the planet and the need for deeper direct-imaging data. In this Letter, we report H-(1.7 μm) and K_1-(2.05 μm) band detections of HD 95086 b from Gemini Planet Imager (GPI) commissioning observations taken by the GPI team. The planet position in both spectral channels is consistent with the NaCo measurements and we confirm it to be comoving. Our photometry yields colors of $H - L' = 3.6 \pm 1.0$ mag and $K_1 - L' = 2.4 \pm 0.7$ mag, consistent with previously reported 5-σ upper limits in H and Ks. The photometry of HD 95086 b best matches that of 2M 1207 b and HR 8799 cde. Comparing its spectral energy distribution with the BT-SETTL and LESIA planet atmospheric models yields $T_{\rm eff} \sim 600$–1500 K and $\log g \sim 2.1$–4.5. Hot-start evolutionary models yield $M = 5 \pm 2\,M_{\rm Jup}$. Warm-start models reproduce the combined absolute fluxes of the object for $M = 4$–14 $M_{\rm Jup}$ for a wide range of plausible initial conditions ($S_{\rm init} = 8$–13 $k_{\rm B}$/baryon). The color−magnitude diagram location of HD 95086 b and its estimated $T_{\rm eff}$ and $\log g$ suggest that the planet is a peculiar L−T transition object with an enhanced amount of photospheric dust.

Key words. planets and satellites: atmospheres – planets and satellites: detection – stars: individual: HD 95086 – instrumentation: adaptive optics

1. Introduction

HD 95086 b is a directly imaged planet ($5 \pm 2\,M_{\rm J}$, $a_{\rm proj} = 55.7 \pm 2.5$ AU) discovered by Rameau et al. (2013a) in L' (3.8 μm) with VLT/NaCo (Lenzen et al. 2003; Rousset et al. 2003) orbiting the young A8 star HD 95086 ($M \sim 1.6\,M_\odot$), a member of the Lower Centaurus Crux subgroup (17 $\pm$ 4 Myr, Pecaut et al. 2012; Meshkat et al. 2013). Additional L' images taken later in 2013 confirmed that the object is comoving with its star (Rameau et al. 2013b).

NaCo Ks (2.18 μm) and NICI (Chun et al. 2008) H-band (1.65 μm) observations failed to reveal the planet (Rameau et al. 2013a; Meshkat et al. 2013). However, 5σ lower limits of Ks-$L' = 1.2 \pm 0.5$ mag and $H - L' = 3.1 \pm 0.5$ mag suggest that the planet may have extremely red colors, similar to the young planets HR 8799 bcde and 2M 1207 b (Chauvin et al. 2004; Marois et al. 2008, 2010a), which have very dusty/cloudy atmospheres (Barman et al. 2011; Currie et al. 2011). Higher contrast near-IR data able to detect HD 95086 b can provide better comparisons with these objects and better constrain its atmosphere.

In this Letter, we present detections of HD 95086 b with the recently installed Gemini Planet Imager (GPI, Macintosh et al. 2014) on Gemini South from public data as a part of GPI commissioning observations (Perrin et al. 2014). The data (acquired and reduced by the GPI team), their analysis, and the detections are presented in Sect. 2. In Sect. 3, we combine GPI H and K_1 photometry with NaCo L' photometry to constrain the physical properties of HD 95086 b.

2. Observations and data reduction

The GPI is a new instrument for imaging and characterizing planets around young nearby bright stars, combining an extreme adaptive optics system, coronagraphs, and an integrated field spectrograph (IFS). The IFS platescale is 14.3 ± 0.3 mas px^{-1} for a 2.8″ field-of-view (FOV) and the true North position angle is given within 1 deg[1].

The HD 95086 spectral data were obtained at H (1.5−1.8 μm, $R = 44$–49) and K_1 (1.9−2.19 μm, $R = 62$–70) in 2013 December using apodized Lyot coronagraphs (Table 1) and angular differential imaging (ADI, Marois et al. 2006a). Conditions were good: 0.43″ and 0.6″ DIMM seeing, air masses of 1.32 and 1.34, and coherence times of 19 ms and 17 ms, respectively. The GPI commissioning team used their pipeline for bad-pixel removal, destriping, non-linearity and persistence corrections, flat-fielding, wavelength calibration, and converting the data into spectral data cubes. We used the data cubes relying on the GPI pipeline quality. The data are made of 21 and 17 spectral

---

[1] http://planetimager.org/

Table 1. Observing log of HD 95086 with GPI.

Date	Filter	Coro mask diam (mas)	DIT(s) × NDITS × Nb_λ	Nb images	FOV rotation (°)
2013/12/10	K_1-coro	306	119.29278 × 1 × 37	17	11.7
2013/12/11	H-coro	246	119.29278 × 1 × 37	21	15.0

Notes. Date, filter, occulting mask diameter, exposure, numbers of coadds, of spectral channels, of images, and FOV rotation.
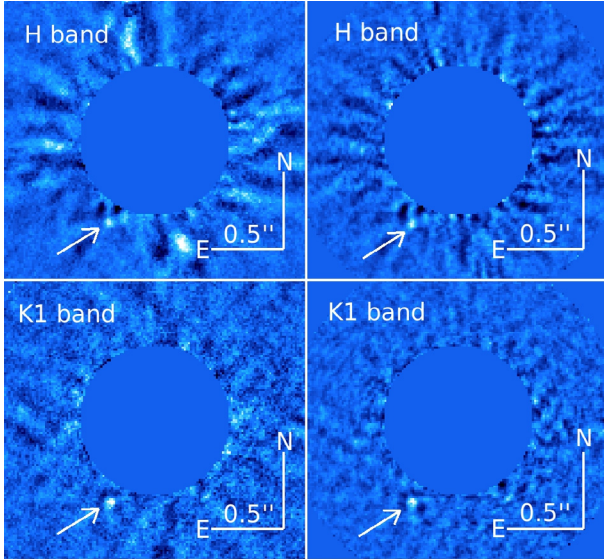

Fig. 1. Final images of the HD 95086 system at H (*top*) and K_1 (*bottom*) bands from two of our pipelines. The planet (arrow) is detected in all images. The bright speckles are masked up to 500 mas from the central star.
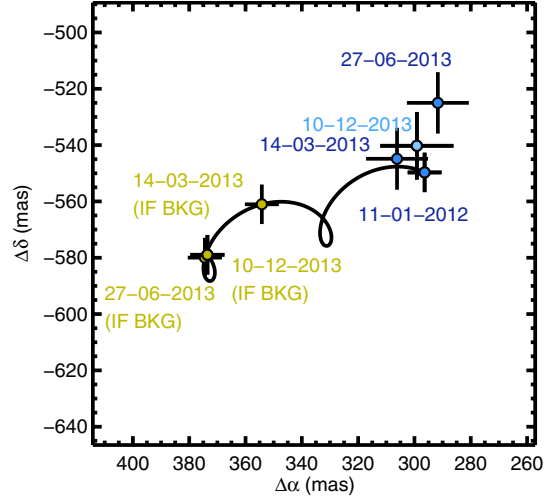

Fig. 2. HD 95086 b positions from its star in RA ($\Delta\alpha$) and Dec ($\Delta\delta$). GPI and NaCo measurements are marked in blue and expected positions of a background object in yellow.

cubes at H and K_1 bands, respectively, consisting of 37 spectral channels each.

To further process the data, we registered each slice of the spectral cubes using the barycenter of the four satellite spots (attenuated replica of the central star PSF induced by a grid placed in a pupil plane, Marois et al. 2006b). Then, we minimized the speckle noise in each slice using independent pipelines each adopting various methods (Marois et al. 2006a; Lafrenière et al. 2007; Lagrange et al. 2010; Boccaletti et al. 2012; Chauvin et al. 2012; Soummer et al. 2012; Currie et al. 2013; Marois et al. 2014) used for ADI and spectral differential imaging (SSDI, Racine et al. 1999). Finally, all slices were mean-combined to yield an integrated broad-band image to maximize the signal-to-noise ratio (S/N) of any off-axis source. Binning images in wavelength and suppressing the speckles (ADI), or suppressing the speckles in each spectral channel (ADI/ADI+SSDI) and binning images give similar results, and all our pipelines recover HD 95086 b, which is the sole bright spot at the expected separation. Thus, we provide the first detections at H and K_1 bands (Fig. 1) with an S/N of ∼3–4 and 5–6, respectively. The central bright speckles are masked up to 500 mas. These are the first detections of HD 95086 b with an instrument that is not NaCo/VLT. No spectrum can be extracted given the low S/N.

To estimate the planet flux and position, we needed unsaturated GPI PSFs. As GPI cannot acquire off-axis observations of the star, we calibrated photometry and astrometry using the satellite spots, which are expected to have same shape and brightness for a given filter. In the laboratory the spot-to-central-star flux ratios were 2.035×10^{-4} (9.23 mag)

and 2.695×10^{-4} (8.92 mag) at H and K_1 bands[1]. To check these values, we compared H and K photometry of HD 8049 B (VLT/ NACO-SINFONI, Zurlo et al. 2013) with our measurements derived from public GPI HD 8049 data. Assuming that the object is not photometrically variable with time and considering the laboratory spot contrasts, GPI and VLT photometry are consistent within $\epsilon_1 = 0.2$ mag, which we take as the error on the ratios. From these ratios, we assessed biases induced by our processing by injecting fake point-sources (i.e., unsaturated PSFs) into the data before applying speckle-suppression techniques (Lagrange et al. 2010; Marois et al. 2010b; Chauvin et al. 2012; Galicher et al. 2012). We obtained templates of the planet image. Adjusting the flux of the templates, we found the planet photometry and the fitting error ϵ_2, which depends on the detection quality. ϵ_2 is 0.8 mag and 0.3 mag at H and K_1. Finally, we estimated the variation ϵ_3 of stellar flux over the sequence with the variation of spot flux. ϵ_3 is 0.2 mag and 0.3 mag over the H and K_1 sequences including the variations between spots. The resulting photometric error is the quadratic error, which is dominated by the low S/N at H and is a mix of all errors at K_1.

For the astrometric error, we considered uncertainties in the centroiding accuracy of individual slices (≤0.3 pixel), the plate scale (0.02 pixel), the planet template fit (0.7 pixel at H, 0.5 pixel at K_1), and the North position angle (1 deg). The error is dominated by the low S/N of the detections and the generic GPI calibrations. The current precision is good enough to assess the comoving status of the companion (Fig. 2). We tried to use the astrometric standard HD 8049 B in GPI data to better constrain the North orientation. We did not succeed because of the high orbital motion of HD 8049 B and because there is no contemporary observation from other instruments.
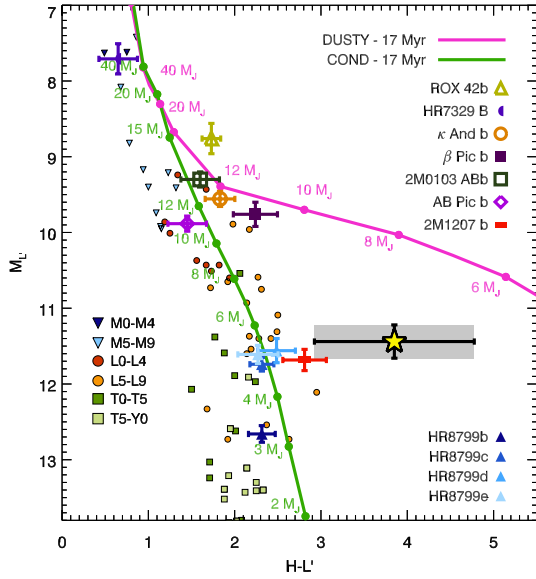
Fig. 3. Color–magnitude diagram using the new *H*-band photometry of HD 95086 b (yellow star) and data from Bonnefoy et al. (2013), Bonnefoy et al. (2014), and Currie et al. (2014).

Table 2. HD 95086 b photometry and astrometry at *H* and K_1 (GPI data) and *L′* (Rameau et al. 2013a,b, and revision*).

Date	Filter	Sep (mas)	PA(°)	Δm
2013/12/11	*H*	633 ± 17	150.6 ± 1.7	13.1 ± 0.9
2013/12/10	K_1	623 ± 15	151.4 ± 1.5	12.1 ± 0.5
2013/03/24	*L′*	626.1 ± 12.8	150.7 ± 1.3	9.71 ± 0.56
2012/01/11	*L′*	623.9 ± 7.4	151.8 ± 0.8	9.79 ± 0.40
2012/01/11	*L′*	623.9 ± 7.4	151.8 ± 0.8	9.48 ± 0.19*

Notes. (*) See text for details.

Final measurements are presented in Table 2. We include revised 2012 NaCo *L′* photometry obtained by 1) better calibrating the planet signal (as in Currie et al. 2013) and 2) precisely deriving the *L′* neutral density (ND) filter throughput (used to flux-calibrate HD 95086) by comparing ND and unsaturated *β* Pic data.

3. Characterization

Absolute magnitudes were derived from the contrast ratios (Table 2): $M_H = 15.29 \pm 0.91$ mag, $M_{K_1} = 14.11 \pm 0.51$ mag, and $M_{L'} = 11.44 \pm 0.22$ mag using the 2MASS and WISE W1 (Cutri et al. 2003, 2012) photometry of the star[2].

Combining the *H* band GPI data with revised NaCo *L′* data, we compared the $L'/H - L'$ color–magnitude diagram position of HD 95086 b with that of young companions, field dwarfs (Leggett et al. 2010, 2013), and LYON evolutionary tracks (Chabrier et al. 2000; Baraffe et al. 2003) generated for the GPI/NaCo passbands[3].

We converted the GPI measurements into H photometry by applying correction factors derived from published spectra, the filter transmissions, and a spectrum of Vega. HD 95086 b lies at

---

[2] Correction factors from the GPI/NaCo and 2MASS/WISE photometry, derived from the spectrum of an A7III star in the Pickles et al. (1998) library, are negligible.

[3] http://phoenix.ens-lyon.fr/simulator/index.faces

Table 3. Physical parameters predicted by hot-start evolutionary models for the observed absolute magnitudes.

	SED		*L′*	
Model	BT-SETTL	Lesia	Dusty	Cond
$T_{\rm eff}$ (K)	1050^{+450}_{-450}	1200^{+300}_{-300}	916^{+43}_{-44}	1108^{+66}_{-65}
log *g* (dex)	$4.0^{+0.5}_{-0.5}$	$3.3^{+1.2}_{-1.2}$	$3.8^{+0.1}_{-0.1}$	$3.9^{+0.1}_{-0.1}$
M ($M_{\rm Jup}$)	–	–	4.5^{+1}_{-1}	$5.5^{+1.5}_{-1.5}$

the *L−T* transition in this diagram, similar to other young (8–30 Myr) planets like HR 8799 cde (Marois et al. 2008, 2010a) and 2M1207 b (Chauvin et al. 2004). Its red $H - L'$ color compared with the sequence of field dwarf objects (Leggett et al. 2010, 2013) suggests a high content of photospheric dust (Barman et al. 2011; Currie et al. 2011), owing to reduced surface gravity (e.g. Fig. 11 of Marley et al. 2012).

We built the 1.5–4.8 μm spectral energy distribution (SED) of the planet following Bonnefoy et al. (2013) by combining the GPI photometry with the *L′* one. The normalized SED (at *L′*) is best compatible with the young exoplanets HR 8799 bcde and 2M1207 b, but is redder. Its colors are also ∼1 mag redder than those of the benchmark dusty L6.5−L7.5 field dwarf 2MASS J22443167+2043433 (Dahn et al. 2002; Stephens et al. 2009).

We also compared the SED of HD 95086 b with the predictions from grids of synthetic spectra for BT-SETTL (Allard et al. 2012) and LESIA atmospheric models (Baudino et al. 2014). Each synthetic SED was normalized to that of HD 95086 b at *L′*. The BT-SETTL grid covers 400 K $\leq T_{\rm eff} \leq$ 3500 K with 50 to 100 K increments, $-0.5 \leq$ log g $\leq$ 6.0 dex with 0.5 dex increments, and M/H = 0.0 or +0.5 dex. The BT-SETTL models that reproduce the photometry of HD 95086 b have 600 K $\leq T_{\rm eff} \leq$ 1500 K and 3.5 dex $\leq$ log *g* $\leq$ 4.5 dex. The three LESIA grids assume 700 K $\leq T_{\rm eff} \leq$ 2100 K, $2.1 \leq$ log g ≤ 4.5 dex, and solar abundances: one without clouds and two with clouds of Fe and Mg_2SiO_4 particles. For each LESIA model, we selected the planet radius that minimizes χ^2 between the observed and calculated apparent magnitudes. We only kept models with a radius in a realistic range derived from evolution models (0.6 to 2 Jupiter radii, Mordasini et al. 2012). All LESIA models that reproduced the HD 950866 b photometry have 900 K $\leq T_{\rm eff} \leq$ 1500 K and 2.1 dex $\leq$ *log g* $\leq$ 4.5 dex.

The planet mass cannot be derived from the atmosphere models, and evolutionary models are needed. Comparing the planet's *L′* luminosity with hot-start DUSTY and COND models for an age of 17 ± 4 Myr, we find a planet mass of $M = 5 \pm 2\,M_{\rm Jup}$ (Table 3). We did not use the *H* and K_1 photometries because they are poorly reproduced by the models for an object at the *L−T* transition (larger uncertainties than for *L′*). The models predict $T_{\rm eff}$ and log *g*, in agreement with those derived from the SED fit.

Alternatively, we used the warm-start models (Spiegel & Burrows 2012) to account for possible different initial conditions for the planet (parameterized by the initial entropy between 8 and 13 $k_{\rm B}$/baryon). The models assume solar metallicity and atmospheres enriched by a factor of 3 with/without dust clouds as boundary conditions. Synthetic SEDs are generated from predicted spectra of planets[4]. For the full range of initial entropies we considered, models assuming masses of 4−14 $M_{\rm Jup}$
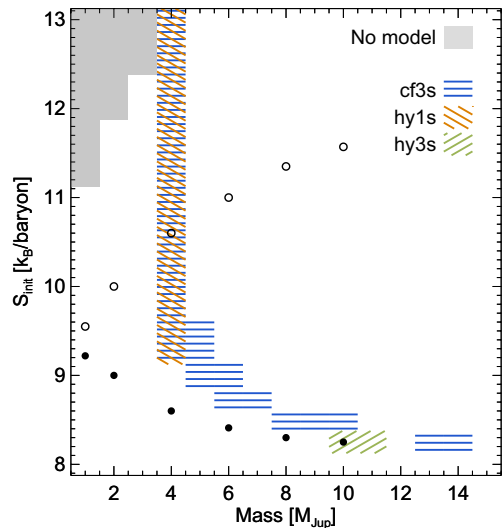
---

[4] http://www.astro.princeton.edu/~burrows/warmstart/spectra.tar.gz

Fig. 4. Combination of initial entropies (S_{init}) and masses (shaded areas) for which the planet 1.6–4.8 μm photometries are reproduced by the warm-start models of Spiegel & Burrows (2012) within 1σ. Three boundary conditions are considered: with (hy) and without (cf) cloudy atmospheres, at solar (1s) and 3x solar (3s) metallicity. Initial entropies for the cold-start (filled circles) and hot-start (open circles) models of Marley et al. (2007) are overlaid.

match the SED of HD 95086 b (Fig. 4). For much of this range ($S_{init} = 9.5-13$) a mass of 4 M_{Jup} is favored.

4. Conclusions

We reported the near-IR detections of HD 95086 b from GPI public commissioning data. We confirmed that the companion is comoving with HD 95086 and derived the first estimates of its magnitudes with respect to its star: $H = 13.1 \pm 0.9$ and $K_1 = 12.1 \pm 0.5$.

While the mid-IR luminosity of HD 95086 b is best consistent with an $L-T$ transition object, it has redder near-IR colors than other young, imaged planet-mass companions. This is consistent with a very dusty and low surface gravity atmosphere.

Comparison with atmosphere models provided $600\,\text{K} \leq T_{eff} \leq 1500\,\text{K}$ and $2.1\,\text{dex} \leq \log g \leq 4.5\,\text{dex}$. Evolutionary models are consistent with a mass of $5 \pm 2\,M_{Jup}$. However, the models are affected by systematic errors that are difficult to quantify because of the lack of young objects at the $L-T$ transition.

More higher-precision spectroscopic and photometric data for HD 95086 b are required to refine the planet properties.

References

Allard, F., Batten, A., Budding, E., et al. 2012, IAU Proc. 282, eds. M. T. Richards, & I. Hubeny, 235
Baraffe, I., Chabrier, G., Barman, T., Allard, F., & Hauschildt, P. 2003, A&A, 402, 701
Barman, T., Macintosh, B., Konopacky, Q. M., & Marois, C. 2011, ApJ, 735, L39
Baudino, J.-L., Brézard, B., Boccaletti, A., Bonnefoy, M., & Lagrange, A.-M. 2014, IAU Proc., 299, 277
Boccaletti, A., Augereau, J.-C., Lagrange, A.-M., et al. 2012, A&A, 544, A85
Bonnefoy, M., Boccaletti, A., Lagrange, A.-M., et al. 2013, A&A, 555, A107
Bonnefoy, M., Chauvin, G., Lagrange, A.-M., et al. 2014, A&A, 562, A127
Chabrier, G., Baraffe, I., Allard, F., & Hauschildt, P. 2000, ApJ, 542, 464
Chauvin, G., Lagrange, A.-M., Dumas, C., et al. 2004, A&A, 425, 29
Chauvin, G., Lagrange, A.-M., Beust, H., et al. 2012, A&A, 542, A41
Chun, M., Toomey, D., Wahhaj, Z., et al. 2008, Proc. SPIE, 7015, 70151
Currie, T., Burrows, A., Itoh, Y., et al. 2011, ApJ, 729, 128
Currie, T., Burrows, A., Madhusudhan, N., et al. 2013, ApJ, 776, 15
Currie, T., Daemgen, S., Debes, J. H., et al. 2014, ApJ, 780, L30
Cutri, R., Skrutskie, M., Van Dyk, S., et al. 2003, VizieR On-line Data Catalog: II/246
Cutri, R., Skrutskie, M., Van Dyk, S., et al. 2012, VizieR On-line Data Catalog: II/311
Dahn, C., Harris, H., Vrba, F., et al. 2002, ApJ, 124, 1170
Galicher, R., & Marois, C. 2012, Proc. of the AO4ELT conference, 25
Lafrenière, D., Marois, C., Doyon, R., Nadeau, D., & Artigau, É. 2007, ApJ, 660, 770
Lagrange, A.-M., Bonnefoy, M., Chauvin, G., et al. 2010, Science, 329, 57
Leggett, S., Burningham, B., Saumon, D., et al. 2010, ApJ, 710, 1627
Leggett, S., Morley, C., Marley, M., et al. 2013, ApJ, 763, 130
Lenzen, R., Hartung, M., Brandner, W., et al. 2003, Proc. SPIE, 4841, 944
Marley, M., Fortney, J., Hubickyj, O., Bodenheimer, P., & Lissauer, J. 2007, ApJ, 655, 541
Marley, M., Saumon, D., Cushing, M. et al. 2012, ApJ, 754, 135
Marois, C., Lafrenière, D., Doyon, R., Macintosh, B., & Nadeau, D. 2006a, ApJ, 641, 556
Marois, C., Lafrenière, D., Macintosh, B., & Doyon, R. 2006b, ApJ, 647, 612
Marois, C., Macintosh, B., Barman, T., et al. 2008, Science, 322, 1348
Marois, C., Macintosh, B., & Véran, J.-P. 2010a, Proc. SPIE, 7736, 77361
Marois, C., Zuckerman, B., Konopacky, Q., et al. 2010b, Nature, 468, 1080
Marois, C., Correia, C., Véran, J.-P., & Currie, T. 2014, IAU Symp., 299, 48
Macintosh, B., Graham, J., Ingraham, P., et al. 2014, PNAS, accepted [arXiv:1403.7520]
Meshkat, T., Bailey, V., Rameau, J., et al. 2013, ApJ, 775, L40
Mordasini, C., Alibert, Y., Georgy, C., et al. 2012, A&A, 547, A112
Pecaut, M.-J., Mamajek, E. E., & Bubar, E. J. 2012, ApJ, 746, 154
Perrin, M., & GPI Instrument and Science teams 2014, AAS Meeting Abstracts, 223, 348
Pickles 1998, PASP, 110, 863
Racine, R., Nadeau, D. & Doyon, R. 1999, ESO Conf. Proc., 56, 377
Rameau, J., Chauvin, G., Lagrange, A.-M., et al. 2013a, ApJ, 772, L15
Rameau, J., Chauvin, G., Lagrange, A.-M., et al. 2013b, ApJ, 779, L26
Rousset, G., Lacombe, F., Puget, P., et al. 2003, Proc. SPIE, 4839, 140
Soummer, R., Pueyo, L., & Larkin, J. 2012, ApJ, 755, L28
Spiegel, D., & Burrows, A. 2012, ApJ, 745, 174
Stephens, D., Leggett, S., Cushing, M., et al. 2009, ApJ, 702, 154
van Leeuwen, F. 2007, A&A, 474, 653
Zurlo, A., Vigan, A., Hagelberg, J., et al. 2013, A&A, 554., A21